Extra large pore opening CFI and DON-type zeosils for mechanical energy storage

Laura Ronchi, Andrey Ryzhikov, Habiba Nouali, T. Jean Daou, Sébastien Albrecht, Joël Patarin

Extra large pore opening CFI and DON-type zeosils for mechanical energy storage

Laura Ronchi [a], Andrey Ryzhikov [a], Habiba Nouali [a], T. Jean Daou [a], Sébastien Albrecht [b], Joël Patarin [a,*]

[a] Université de Strasbourg (UDS), Université de Haute Alsace (UHA), Axe Matériaux à Porosité Contrôlée (MPC), Institut de Science des Matériaux de Mulhouse (IS2M), UMR CNRS 7361, 3 bis rue Alfred Werner, F-68093 Mulhouse, France
[b] Université de Strasbourg (UDS), Université de Haute Alsace (UHA), Laboratoire de Chimie Organique et Bioorganique (COB), EA 4566, ENSCMu, F-68093 Mulhouse, France

A B S T R A C T

The energetic performances of pure silica CFI and DON-type zeolites (zeosils) were studied by intrusion-extrusion experiments in water and LiCl aqueous solutions at different concentrations. For both zeosils, characterized by a 1D channel system with 14 MR pore openings, when water is used as nonwetting liquid a perfect reversible spring behavior is observed with an intrusion pressure of 75 and 26 MPa, respectively. The lower value for the DON-type structure is probably due to a larger pore aperture. The intrusion pressures in both cases rise considerably with the LiCl concentration, but the doubling of the salt concentration from 10 to 20 M leads only to a slight increase of the intrusion pressure. The maximal stored energy achieves 14.6 and 6.8 J/g for CFI and DON-type zeosil-based systems, respectively. The zeolite samples were characterized before and after intrusion-extrusion experiments by XRD, SEM, N_2 adsorption-desorption, TG and NMR analysis in order to get a better understanding of the influence of these intrusion-extrusion experiments on the CFI and DON-type structures.

1. Introduction

Zeolites are crystalline microporous solids widely used in adsorption, molecular separation, ion-exchange and catalysis processes [1]. In 2001 a peculiar application has been developed by our group for pure silica zeolites (zeosils) in the energy field [2]. Indeed the hydrophobic character of these materials is exploited for mechanical energy storage and dissipation by forcing the intrusion of water inside the pores of these solids under high pressure. During the penetration into the pores (intrusion), the supplied mechanical energy is converted into solid-liquid interfacial energy. Depending on the particular features of the considered zeosil (dimensionality of the porous system, type of porosity (channel or cage), presence of defects, …), when the pressure is released (extrusion) the "zeosil-water" system can restore, dissipate or absorb the supplied energy showing, therefore a spring, a shock-absorber or a bumper behavior. Various "zeosil-water" systems have already been studied by our group [2–4] and a relationship between the type of porosity and the intrusion pressure was established [5].

In recent years, it has been proved that replacing water with electrolyte solutions leads to an increase of the intrusion pressure, improving therefore the energetic performances of the corresponding "zeolite-nonwetting liquid" system [6–12]. For instance, the intrusion pressure can be enhanced by 7.4 times using a 20 M LiCl aqueous solution instead of pure water on a LTA-type zeosil based system [7].

In this work and for the first time a focus is made on the energetic performances of pure silica CFI and DON-type zeolites with extra-large pore openings (hereafter, Si-CFI and Si-DON). They are both characterized by a one-dimensional (1D) channel system with 14 MR (membered ring) openings [13,14]. The first one ever synthesized was UTD-1 (DON-type) [14] using the organometallic complex (bis (pentamethylcyclopentadienyl)cobalt(III)) hydroxide, $[(Cp^*)_2Co]OH$ as structure-directing agent. In the following years other high silica extra-large pore zeolites were synthesized such as CIT-5 (CFI-type) [13,15], SSZ-53 (SFH-type) [16] and SSZ-59 (SFN-type) [16]. These zeolites were developed to extend the research in the adsorption and catalysis fields [13,16].

* Corresponding author.
E-mail address: joel.patarin@uha.fr (J. Patarin).

Until now, various one-dimensional channel-type zeosils (AFI, MTT, MTW and TON) [3,17] with smaller pore openings (10 or 12 MR) were tested for water intrusion. An interesting remark is that despite a formal smaller pore opening (12 MR), the AFI-type zeosil displays a pore aperture similar to the CFI-type one (7.3×7.3 Å^2) and (7.2×7.5 Å^2), respectively [18]. This feature makes the comparison of the "AFI and CFI-water" systems interesting. The pore size of the DON-type zeosil is larger (8.1×8.2 Å^2).

In the present work, the energetic performances of the "Si-CFI-nonwetting liquid" and Si-DON-nonwetting liquid" systems are reported. Water and LiCl aqueous solutions at two different concentrations (10 M and 20 M) are chosen as nonwetting liquids. The samples were fully characterized before and after intrusion-extrusion experiments by powder X-ray diffraction, Scanning Electron Microscopy, thermal analysis, N_2 adsorption-desorption and solid-state NMR spectroscopy in order to study the influence of these experiments on the zeosil structures.

2. Experimental section

2.1. Synthesis of Si-CFI and Si-DON samples

The Si-CFI sample was synthesized in fluoride medium according the procedure published by Barrett et al. [13] using N-methyl-(−)-sparteinium in the hydroxide form as structure-directing agent (SDA(OH)). The reactants used were: tetraethylorthosilicate (Evonik) as silica source, SDA(OH) (homemade synthesis, see Supporting Information) and HF ≥ 40 wt % (Sigma-Aldrich). The starting gel (molar composition: 1 SiO_2: 0.5 SDA(OH): 0.5 HF: 15 H_2O) was introduced in a Teflon-lined stainless-steel autoclave and heated at 175 °C during 11 days under stirring at 60 rpm. After synthesis, the product was filtered, washed with distilled water and ethanol, then dried in an oven at 70 °C overnight. At the end, the solid was calcined at 650 °C under air for 3 h to completely remove the organic template.

The Si-DON sample was synthesized according to an adapted procedure published by Freyhardt et al. [14] using [(Cp*)$_2$Co]OH as structure-directing agent (SDA(OH)). The reactants used were: fumed silica (Cab-O-Sil M5) as silica source, NaOH > 97 wt % (Carlo Erba) and bis(pentamethylcyclopentadienyl)cobalt(III) hexafluorophosphate (Alfa Aesar, 98%) as SDA in its hydroxide form (see Supporting Information). The starting gel (molar composition: 1 SiO_2: 0.13 SDA(OH): 0.09 NaOH: 57 H_2O) was introduced in a Teflon-lined stainless-steel autoclave and heated at 150 °C during 14 days. After synthesis, the product was filtered, washed with distilled water and ethanol, then dried in an oven at 70 °C overnight. In order to remove the organometallic template, the solid was previously calcined at 550 °C under air for 6 h, then treated with a 12 M HCl aqueous solution for 2 h at room temperature and afterwards with a 7 M HCl one at 50 °C overnight.

2.2. Intrusion–Extrusion experiments

The intrusion-extrusion of water and LiCl aqueous solutions was performed at room temperature using a Micromeritics mercury porosimeter (Model Autopore IV), as described in a previous work [19].

Prior to the analyses, the Si-CFI and Si-DON samples (non-intruded and intruded-extruded ones) were hydrated in a 80% relative humidity atmosphere for 24 h in order to set the hydration state.

2.3. Powder X-ray diffraction

Powder X-ray diffraction patterns of the different samples were recorded on a STOE STADI-P diffractometer in the transmission scan mode equipped with a curved germanium (111), primary monochromator and a linear position-sensitive detector (6° 2θ) using CuKα_1 radiation (λ = 0.15406 nm). Measurements were achieved for 2θ angle values in the 3–50° range step 0.2° 2θ and time/step = 10 s.

2.4. Scanning electron microscopy

The size and the morphology of the crystals were determined by scanning electron microscopy (SEM) using a Philips XL 30 FEG microscope.

2.5. Nitrogen Adsorption–Desorption measurements

Nitrogen adsorption–desorption isotherms were performed at 77 K using a Micromeritics ASAP 2420 apparatus. Prior to the adsorption measurements, the nonintruded sample were outgassed at 90 or 300 °C overnight under vacuum. The intruded–extruded samples were outgassed at 90 °C overnight to avoid the dehydroxylation process. The specific surface area and microporous volume (V_{micro}) were calculated using the BET and t-plot methods, respectively.

2.6. Thermal analysis

Thermogravimetric (TG) analyses were carried out on a Mettler Toledo STARe apparatus, under air flow, with a heating rate of 5 °C/min from 30 to 800 °C.

2.7. Solid-state NMR spectroscopy

^{29}Si MAS and ^{1}H–^{29}Si CPMAS NMR spectra were recorded at room temperature on a Bruker Advance II 300 MHz spectrometer, with a double-channel 7 mm Bruker MAS probe. The recording conditions are given in Table 1.

3. Results and discussion

3.1. Intrusion-extrusion experiments

For all the systems, three intrusion-extrusion cycles were performed. For clarity only the first two cycles are presented, because all the cycles are superimposable. The 0–5 MPa range on the pressure-axis is not shown, since the observed volume variation is due to the intrusion of the nonwetting liquid in the interparticular porosity of the zeosil pellet, as already mentioned in our previous work [4].

Table 1
Recording conditions of the ^{29}Si MAS and ^{1}H-^{29}Si CPMAS NMR spectra.

	^{29}Si MAS	^{1}H-^{29}Si CPMAS
Chemical Shift Standard	TMS[a]	TMS[a]
Frequency (MHz)	59.6	59.6
Pulse width (μs)	2.3	5.0
Flip angle	π/6	π/2
Contact time (ms)	/	1
Recycle time (s)	80	[b] 3
Spinning rate (kHz)	4	4
Scans number	1500	15,000

[a] Tetramethylsilane.
[b] The relaxation time t_1 was optimized.

3.1.1. "Si-CFI-nonwetting liquid" system

The pressure-volume diagrams of the "Si-CFI-water" and "Si-CFI-LiCl aqueous solutions" systems are shown in Fig. 1. The corresponding characteristic data are reported in Table 2.

The pressure-volume diagrams depicted in Fig. 1 show that for the "Si-CFI-water" system the intruded liquid at 75 MPa is completely expelled at the same pressure from the porous matrix when the pressure is released. This indicates that the system is a perfect spring that can store and restore an energy of 6.0 J/g over several cycles. The intruded volume (0.08 mL/g) is lower than the porous volume determined by N_2 adsorption-desorption measurements (0.13 cm^3/g, see Table 3), but the difference is consistent with the one previously found for Silicalite-1 by Desbiens et al. [20], where the water density inside the zeolite porosity must be corrected at 0.6 instead of the usual 1.0.

Comparing the energetic performances of the "Si-CFI-water" system with the ones of other "one-dimensional channel-type zeosil-water" systems (AFI, MTT, MTW and TON) [3,17], the same spring behavior is found. The absence of hysteresis between the intrusion and extrusion curves would indicate a very low amount of defect sites (dangling -OH groups) in the intruded-extruded samples as confirmed from TG and NMR analysis.

A previous work showed that the intrusion pressure is determined by the pore window diameter for channel-type zeosils and by the cage diameter for cage-type ones [5]. When intruded with water, TON and MTT-type zeosils, which are characterized by a 10 MR pore opening with similar diameter, show very high intrusion pressure values (186 and 176 MPa, respectively) [3,17]. For zeosils with larger pore openings (12 MR) such as AFI and MTW-type zeosils, water molecules can be more easily intruded into the porosity at 58 and 126 MPa, respectively [3]. The huge difference between the latter values is ascribed to the peculiar large dimension of AFI-type zeosil pore opening, (7.3 × 7.3 $Å^2$) compared to MTW one (5.6 × 6.0 $Å^2$). Since the AFI-type zeosil pore opening is similar to the Si-CFI-type one (7.2 × 7.5 $Å^2$), as expected, the intrusion pressure is observed in the same pressure range (58 and 75 MPa, respectively).

The increase of the LiCl concentration leads to an increase of the intrusion pressure (75, 147 and 162 MPa for water, 10 M and 20 M LiCl aqueous solutions, respectively). Several hypotheses have been proposed to explain such a phenomenon: i) a higher solid-liquid interfacial tension of electrolyte aqueous solution in comparison with water [21,22], ii) an osmotic phenomenon [23,24], iii) a confinement effect of the nanopore walls [10] or iv) a ion desolvation phenomenon [6,25]. A recent study, dealing with the "FER-type zeosil-$MgCl_2 \cdot 21\ H_2O$" system demonstrated that the electrolyte aqueous solution intruded into the pores is more concentrated ($MgCl_2 \cdot 10\ H_2O$) than the initial one. The decrease of the water content and, thus, the higher concentration of the intruded solution could be reasonably the result of the hydrophobic nature of the host zeolite matrix [26].

It can be interesting to compare the intrusion pressure values with those obtained for the systems based on 3D channel-type zeosils. A linear increase (96, 193 and 285 MPa for water, 10 M and 20 M LiCl aqueous solutions, respectively) was observed for the MFI-type zeosil (10 MR) [9], while for the *BEA-type (12 MR) [8] the increase between water and 10 M LiCl aqueous solution is more important than the one between 10 M and 20 M LiCl aqueous solutions (53, 95 and 115 MPa for water, 10 M and 20 M LiCl aqueous solutions, respectively). The same trend than in latter case is observed for the "Si-CFI-nonwetting liquid" systems. This is probably related to the larger pore opening of *BEA-type and CFI-type zeosils that oppose less resistance to the liquid.

For "Si-CFI-LiCl aqueous solutions" systems, the spring behavior with an energy yield of 97% is maintained, but a slight hysteresis is visible. This trend was already observed for MFI-type zeolite [9]. The rise of the intrusion pressure with LiCl aqueous solutions leads to an increase of the stored energy (6.0, 13.2 and 14.6 J/g for water, 10 M and 20 M LiCl aqueous solutions, respectively). Such energy values are relatively low compared to MFI-based systems (31 J/g with 20 M LiCl aqueous solution).

3.1.2. "Si-DON-nonwetting liquid" system

The P-V diagrams of the "Si-DON-nonwetting liquid" systems are reported in Fig. 2 and the corresponding data in Table 2. Compared to the "Si-CFI-nonwetting liquid" system and whatever the nonwetting liquid, the intrusion step is less steep (Fig. 2). An important spread is observed particularly for the LiCl-based

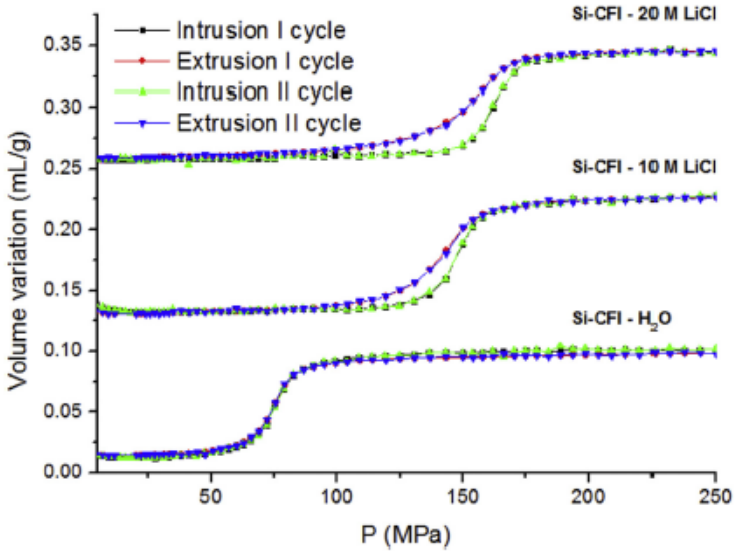

Fig. 1. First and second intrusion-extrusion cycles of the "Si-CFI-water" and "Si-CFI-LiCl aqueous solutions" systems. For clarity, the intrusion-extrusion isotherms are shifted along the Y axis.

Table 2
Characteristics of the Si-CFI and Si-DON based systems: Intrusion (P_{int}) and Extrusion (P_{ext}) Pressures, Intruded (V_{int}) and Extruded (V_{ext}) Volumes, Stored (E_s) and Restored (E_r) Energies after water and LiCl aqueous solution intrusion-extrusion experiments at different LiCl concentrations (10 M and 20 M). These values are the same for the three intrusion-extrusion cycles.

System	P_{int} [MPa][a]	P_{ext} [MPa][a]	V_{int} [ml/g][a]	V_{ext} [ml/g][a]	E_s [J/g][b]	E_r [J/g][c]	Energy Yield (%)[d]
Si-CFI - H_2O	75	75	0.08	0.08	6.0	6.0	100
Si-CFI - 10 M LiCl	147	143	0.09	0.09	13.2	12.9	97
Si-CFI - 20 M LiCl	162	158	0.09	0.09	14.6	14.2	97
Si-DON - H_2O	26	21	0.04	0.04	1.0	0.8	81
Si-DON - 10 M LiCl	81	70	0.06	0.06	4.9	4.2	86
Si-DON - 20 M LiCl	85	75	0.08	0.08	6.8	6.0	88

[a] Determined from intrusion–extrusion curves.
[b] Stored energy $E_s = V_{int} \times P_{int}$.
[c] Restored energy $E_r = V_{ext} \times P_{ext}$.
[d] Energy yield (%) $= E_r/E_s \times 100$.

systems. For instance, the intrusion starts around 25 MPa with a complete filling of the pores at around 150 MPa (20 M LiCl). The crystal morphology (packed needles) might be responsible of the spreading in pressure as previously observed for the TON-type zeosil [3]. However, in all cases a spring behavior is mainly observed with a slight hysteresis between the intrusion and extrusion curves for the "Si-DON-20 M LiCl aqueous solution" system. Although both CFI and DON-type zeosils display a 1D channel system with 14 MR openings, the intrusion pressures for the Si-DON-based systems are strongly lower (from 26 to 85 MPa, see Table 2). Such a result is not so surprising since the pore apertures of the DON-type structure are larger (see introduction section).

The intruded volumes with water and 10 M LiCl aqueous solutions (0.04 and 0.06 mL/g, respectively) are quite low compared to the microporous volume found by N_2 adsorption-desorption measurements (0.15 cm^3/g, see below) and cannot be explained only by the lower density of water confined in the nanopores of the zeolite. Another explanation could be the partially spontaneous intrusion of the liquid inside the porous matrix at low pressure (in the nonreported 0–5 MPa range, see above). For the 20 M LiCl aqueous solution, the intruded volume is higher (0.08 mL/g) revealing thus a non intrusion of this liquid at low pressure. A similar evolution of intruded volume with LiCl concentration was previously observed in the case of high-silica (Si/Al = 110) FAU-type zeolite with partially hydrophobic pores [27]. Unfortunately, despite the large pore openings the stored energy for "Si-DON-nonwetting liquid" systems are low and ranging from 1.0 to 6.8 J/g.

3.2. XRD and SEM characterizations

The XRD patterns of the different Si-CFI and Si-DON samples are reported in Figs. 3 and 4, respectively. For both zeosils no significant changes are observed before and after intrusion-extrusion experiments. This indicates that at the long-range order the structures are not affected by the high pressure experiments.

The Si-CFI and Si-DON samples were also examined by Scanning Electron Microscopy, before and after the intrusion-extrusion cycles. The crystals of the nonintruded Si-CFI sample (Fig. 5a) display a rod shape morphology with dimensions of ~10 × 0.7 × 0.7 μm^3

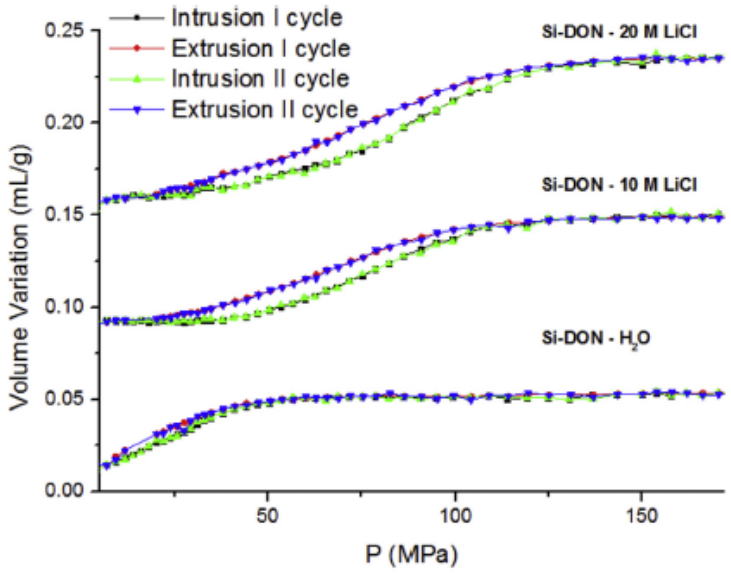

Fig. 2. First and second intrusion-extrusion cycles of the "Si-DON-water" and "Si-DON-LiCl aqueous solutions" systems. For clarity, the intrusion-extrusion isotherms are shifted along the Y axis.

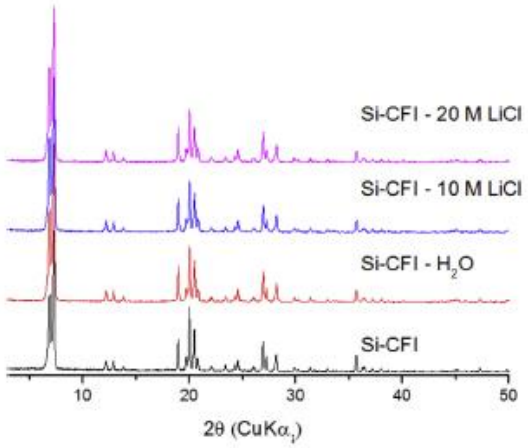

Fig. 3. XRD patterns of Si-CFI samples before and after three intrusion-extrusion cycles in water, 10 M and 20 M LiCl aqueous solutions.

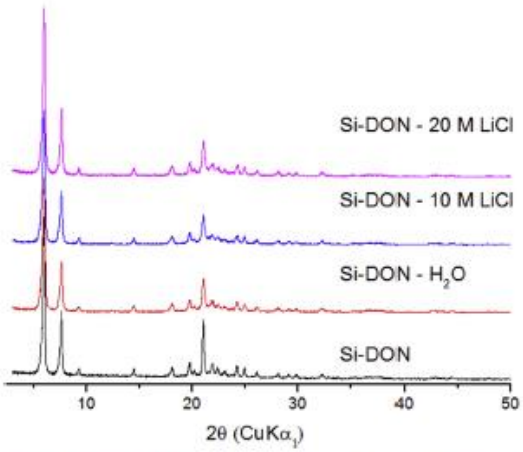

Fig. 4. XRD patterns of Si-DON samples before and after three intrusion-extrusion cycles in water, 10 M and 20 M LiCl aqueous solutions.

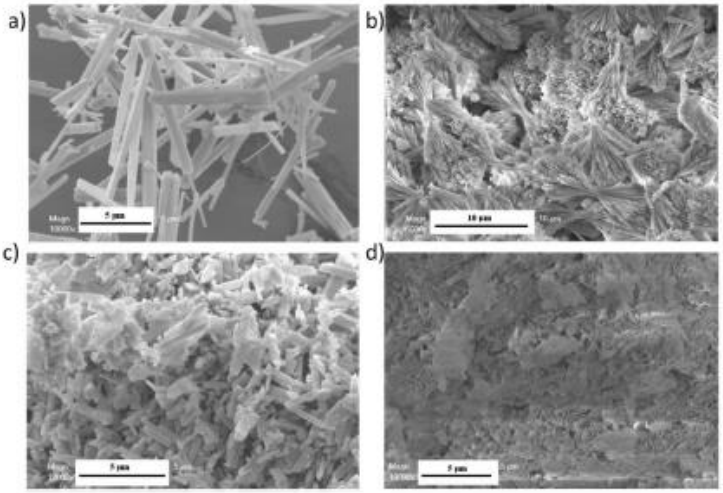

Fig. 5. SEM micrographs of Si-CFI and Si-DON samples before (a and b, respectively) and after three intrusion-extrusion cycles in water (c and d, respectively).

whereas those of Si-DON (Fig. 5b) consist in packed needles of dimensions of ~10 × 0.2 × 0.1 μm^3. In both cases and whatever the nature of the intruded liquid, after intrusion-extrusion experiments the crystals are broken (Fig. 5c and d).

3.3. N_2 adsorption-desorption isotherms

3.3.1. Si-CFI samples

The N_2 adsorption-desorption isotherms of the nonintruded and intruded samples are shown in Fig. 6. In all cases the isotherms are mainly of type I characteristic of microporous solids. The BET surface area and microporous volume (V_{micro}) of the nonintruded sample outgassed at 300 °C are 340 m^2/g and 0.130 cm^3/g, respectively, that are similar to the values reported in the literature [13]. After an outgassing at 90 °C, a lower surface area (245 m^2/g) and a lower microporous volume are observed (0.095 cm^3/g) revealing thus the presence of remaining physisorbed water in the nonintruded sample. After intrusion-extrusion experiments, the pore volume and surface area are considerably lower (see Table 3). All these results are quite in agreement with the TG curves since for all the samples the end of the first weight loss is observed at 150−200 °C and this weight loss, in particular for the LiCl aqueous solutions intruded samples, is larger for the intruded samples (see Fig. 7). The larger amount of physisorbed water in the intruded samples indicates the creation of few hydrophilic defects sites (-OH groups). However, after an outgassing at 300 °C (see Supporting Information, Fig. S1), the microporous volume of the water-intruded sample (0.12 cm^3/g) is comparable with the one of the nonintruded solid confirming that no great damages are caused after intrusion under high pressure as confirmed by NMR spectroscopy.

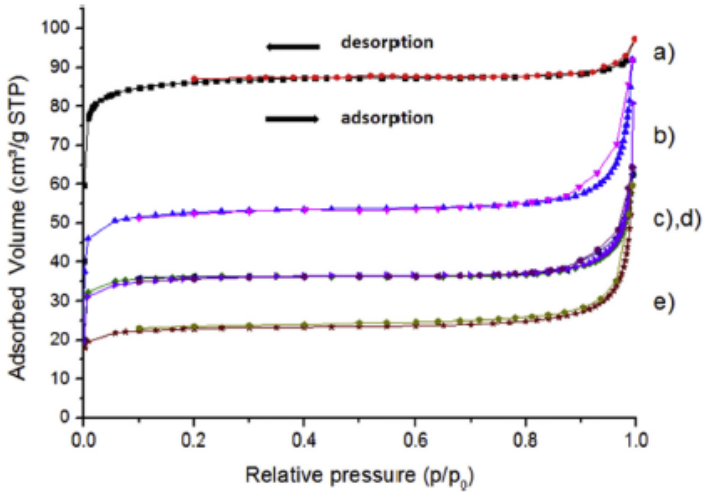

Fig. 6. N_2 adsorption-desorption isotherms at −196 °C of the nonintruded Si-CFI samples outgassed at a) 300 °C and b) 90 °C and Si-CIF samples outgassed at 90 °C after intrusion-extrusion in c) water, d) 10 M and e) 20 M LiCl aqueous solutions.

Table 3
Microporous volume (V_{micro}) and specific surface area S_{BET} values obtained from N_2 adsorption-desorption isotherms at −196 °C of Si-CFI samples before and after intrusion-extrusion experiments outgassed at 90 and 300 °C.

Outgassing temperature	Si-CFI (300 °C)	Si-CFI (90 °C)	Si-CFI-H_2O (90 °C)	Si-CFI-10 M LiCl (90 °C)	Si-CFI-20 M LiCl (90 °C)
V_{micro} (cm^3/g)	0.130	0.095	0.050	0.050	0.035
S_{BET} (m^2/g)	343	245	125	120	95

3.3.2. Si-DON samples

For all Si-DON samples, the N_2 adsorption-desorption isotherms (see Supporting Information, Fig. S2) are mainly of type I and characteristic of microporous solids. The BET surface area and microporous volume of the nonintruded sample outgassed at 300 °C are 408 m^2/g and 0.15 cm^3/g, respectively, while when outgassed at 90 °C they are 252 m^2/g and 0.10 cm^3/g, respectively. Similar characteristic data are obtained for the intruded samples outgassed at 90 °C whatever the nonwetting liquid. Therefore, as for the Si-CFI samples and in agreement with the TG analysis (see Supporting Information, Fig. S3), after an outgassing at 90 °C the microporous volume found for the nonintruded and intruded samples (0.095 cm^3/g in both cases) can be ascribed to the presence of remaining physisorbed water.

3.4. Thermogravimetric analysis

3.4.1. Si-CFI samples

The experimental results issued from the thermogravimetric (TG) analysis of the Si-CFI samples before and after intrusion-extrusion experiments are depicted in Fig. 7. The high hydrophobic character is confirmed by the small total weight loss that ranges from 0.6 wt % for the nonintruded sample to 1.4 wt % for the samples intruded with 10 M and 20 M LiCl aqueous solutions. The weight losses occur in two main steps. The first one, between 30 and 200 °C, is ascribed to the desorption of physisorbed water molecules. The second one, in the temperature range of 200–800 °C, can be assigned to water arising from dehydroxylation reactions. The creation of defects (dangling −OH groups) during the intrusion-extrusion experiments is indicated by the increase of this second weight loss for the intruded samples and therefore the increase of the number of −OH groups per unit cell ($Si_{32}O_{64}$): ~0.5 for the nonintruded sample, ~1.0 for the one intruded with water and ~2.0 for the LiCl aqueous solution intruded ones. However, according to the NMR results (see below), the number of -OH groups per unit cell is still quite low after intrusion-extrusion experiments.

3.4.2. Si-DON samples

Compared to the Si-CFI samples, the total weight loss for the Si-DON samples is higher and ranges from 3.0 wt % for the nonintruded sample to 3.75 wt % for the sample intruded with 20 M LiCl aqueous solution (see Supporting Information, Fig. S3). It also occurs in two main steps corresponding to the removal of physisorbed water molecules and the removal of water arising from dehydroxylation reactions. From the second weight loss, whatever the samples (intruded or nonintruded ones) about 8 -OH groups were found per unit cell ($Si_{64}O_{128}$). From these results, it seems that the intrusion-extrusion experiments do not cause significant damages in the zeosil structure as confirmed by NMR spectroscopy (see below).

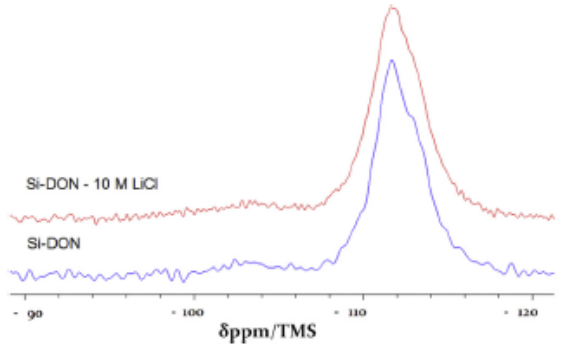

Fig. 10. ^{29}Si-MAS NMR spectra of the Si-DON samples before and after three intrusion-extrusion cycles in 10 M LiCl aqueous solution.

at −102.8 ppm corresponding to Q_3 species (silanol groups) is clearly detected in both spectra. Although the NMR spectrum of the nonintruded sample shows a lower signal/noise ratio, the number of defect sites does not seem to increase after intrusion-extrusion experiments which is in quite good agreement with the TG results (the number of -OH groups for these samples is about 0.5 and 2.0 -OH per unit cell).

3.5.2. Si-DON samples

The ^{29}Si MAS NMR spectra of the Si-DON samples before and after intrusion-extrusion experiments with 10 M LiCl aqueous solution are shown in Fig. 10. In agreement with the literature [29], both spectra exhibit a very broad resonance between −106.6 and −119.2 ppm ascribed to Q_4 groups ($Si-(OSi)_4$) and corresponding to the five non-equivalent crystallographic silicon sites (orthorhombic symmetry) of the framework. Another smaller component, between −97.0 and −106.5 ppm, attributable to Q_3 sites is also visible. It corresponds to about 7.0% of the total ^{29}Si signal, value in quite good agreement with the TG results (8 -OH group per unit cell). From structural characterization of the calcined form of UTD-1, Lobo and coworkers [14,29] showed that the structure was highly faulted and disordered along the one-dimensional 14-ring channel. Such a disorder can explain the presence of the broad Q_4 component on the NMR spectra. No relevant differences can be found between the NMR spectra of the nonintruded and intruded samples. This indicates that at the short-range order the zeolite structure is not affected after the intrusion-extrusion experiments.

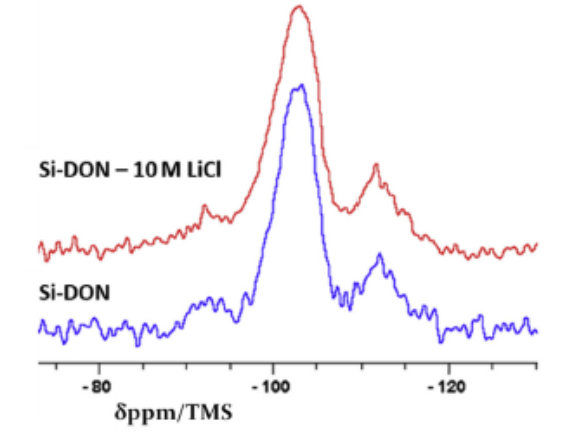

Fig. 11. ^{1}H-^{29}Si-CPMAS NMR spectra of the Si-DON samples before and after three intrusion-extrusion cycles in 10 M LiCl aqueous solution.

The corresponding ^{1}H-^{29}Si CPMAS NMR spectra are shown in Fig. 11. They are very similar and display three components with maxima at −92.6, −103.5 and −112.6 ppm. The latter corresponds to Q_4 groups while the former to Q_2 ($(HO)_2$-Si-$(OSi)_2$) and Q_3 (HO)-Si-$(OSi)_3$) groups. No significant difference is observed between these spectra which means that the impact of intrusion-extrusion experiments on the DON-type structure is very low.

4. Conclusion

The energetic performances of pure silica CFI- and DON-type zeolites were studied by intrusion-extrusion in water and LiCl aqueous solutions at different concentrations. These zeosils are characterized by a one-dimensional channel-system with extra-large pore openings (14 MR), the largest between all studied zeosils for energetic applications. As it was already observed for other water-intruded zeosils with 1D pore system (AFI, MTT, MTW and TON), "Si-CFI-water" and "Si-DON-water" systems show a spring behavior. Because of the larger pore size a quite low value of the intrusion pressure is observed (75 and 26 MPa, respectively) which is comparable with the one found for AFI-type zeosil based system (58 MPa) that have similar pore apertures. The lower value for the DON-type structure can be explained by a larger pore aperture. Using a 10 M LiCl aqueous solution, the intrusion pressure is considerably increased (147 and 81 MPa, respectively), while doubling the LiCl concentration only a slight increase is observed (162 and 85 MPa, respectively). The concentration increase does not affect the spring behavior of the system, but a slight hysteresis between the intrusion and extrusion curves is observed. The different characterization techniques show that intrusion-extrusion experiments induce only a slight amount of defect sites in the zeosils structure. With water and 10 M LiCl aqueous solution, a low intruded volume is observed for DON-type zeosil that can be related with the partially hydrophilic character of its structure. Unfortunately, the stored energy for both CFI and DON-based systems are quite low: 14.6 and 6.8 J/g, respectively, for 20 M LiCl aqueous solution.

Acknowledgements

Laura Ronchi thanks the University of Haute Alsace (UHA) for their financial support for her Ph.D. grant. The authors would like to thank Ludovic Josien, Séverinne Rigolet and Laure Michelin for their assistance in scanning electron microscopy, NMR analyses and XRD measurements.

A special thank to Jean-Louis Paillaud and Minh Hang Au for the synthesis of SDA.

Appendix A. Supplementary data

Supplementary data related to this article can be found at http://dx.doi.org/10.1016/j.micromeso.2017.07.039.

References

[1] J. Čejka, H. Van Bekkum, A. Corma, F. Schüth, Stud. Surf. Sci. Catal. 168 (2007) 1–1047.

[2] V. Eroshenko, R.C. Regis, M. Soulard, J. Patarin, J. Am. Chem. Soc. 123 (2001) 8129–8130.

[3] L. Tzanis, M. Trzpit, M. Soulard, J. Patarin, Microporous Mesoporous Mater 146 (2011) 119–126.

[4] L. Tzanis, B. Marler, H. Gies, J. Patarin, J. Phys. Chem. C 117 (2013) 4098–4103.
[5] L. Tzanis, M. Trzpit, M. Soulard, J. Patarin, J. Phys. Chem. C 116 (2012) 20389–20395.
[6] M. Soulard, J. Patarin, Pat FR2976030 (2012).
[7] A. Ryzhikov, L. Ronchi, H. Nouali, T.J. Daou, J.-L. Paillaud, J. Patarin, J. Phys. Chem. C 119 (2015) 28319–28325.
[8] A. Ryzhikov, I. Khay, H. Nouali, T.J. Daou, J. Patarin, Phys. Chem. Chem. Phys. 16 (2014) 17893–17899.
[9] I. Khay, T.J. Daou, H. Nouali, A. Ryzhikov, S. Rigolet, J. Patarin, J. Phys. Chem. C 118 (2014) 3935–3941.
[10] A. Han, W. Lu, T. Kim, V.K. Punyamurtula, Y. Qiao, Smart Mater. Struct. 18 (2009) 24005.
[11] A. Han, Y. Qiao, J. Mater. Res. 22 (2007) 644–648.
[12] L. Liu, X. Chen, W. Lu, A. Han, Y. Qiao, Phys. Rev. Lett. 102 (2009), 184501-1-4.
[13] P.A. Barrett, M.J. Diaz-Cabañas, M.A. Camblor, R.H. Jones, J. Chem. Soc. Faraday Trans. 94 (1998) 2475–2481.
[14] C.C. Freyhardt, M. Tsapatsis, R.F. Lobo, K.J. Balkus, M.E. Davis, Nature 381 (1996) 295–298.
[15] P. Wagner, M. Yoshikawa, K. Tsuji, M.E. Davis, P. Wagner, M. Lovallo, M. Taspatsis, Chem. Commun. (1997) 2179–2180.
[16] A. Burton, S. Elomari, C.-Y. Chen, R.C. Medrud, I.Y. Chan, L.M. Bull, C. Kibby, T.V. Harris, S.I. Zones, E.S. Vittoratos, Chem. - Eur. J. 9 (2003) 5737–5748.
[17] A. Ryzhikov, I. Khay, H. Nouali, T.J. Daou, J. Patarin, RSC Adv. 4 (2014) 37655–37661.
[18] http://europe.iza-structure.org/IZA-SC/ftc_table.php.
[19] M. Trzpit, M. Soulard, J. Patarin, Chem. Lett. 36 (2007) 980–981.
[20] N. Desbiens, I. Demachy, A.H. Fuchs, H. Kirsch-Rodeschini, M. Soulard, J. Patarin, Angew. Chem. Int. Ed. 44 (2005) 5310–5313.
[21] E.W. Washburn, Proc. Natl. Acad. Sci. U. S. A. 7 (1921) 115–116.
[22] W. Peiming, A. Anderko, R.D. Young, Ind. Eng. Chem. Res. 50 (2011) 4086–4098.
[23] M. Michelin-Jamois, C. Picard, E. Charlaix and G. Vigier, ArXiv:1404.5318v1 Physics.chem-Ph (2014) 1–4.
[24] M. Michelin-Jamois, C. Picard, G. Vigier, E. Charlaix, Phys. Rev. Lett. 115 (2015) 036101/1–036101/4.
[25] A. Han, V.K. Punyamurtula, Y. Qiao, Appl. Phys. Lett. 92 (2008), 153117–1-3.
[26] R. Arletti, L. Ronchi, S. Quartieri, G. Vezzalini, A. Ryzhikov, H. Nouali, T.J. Daou, J. Patarin, Microporous Mesoporous Mater 235 (2016) 253–260.
[27] A. Ryzhikov, I. Khay, H. Nouali, T.J. Daou, J. Patarin, Microporous Mesoporous Mater 221 (2016) 1–7.
[28] M. Yoshikawa, P. Wagner, M. Lovallo, K. Tsuji, T. Takewaki, C.-Y. Chen, L.W. Beck, C. Jones, M. Tsapatsis, S.I. Zones, M.E. Davis, J. Phys. Chem. B 102 (1998) 7139–7147.
[29] R.F. Lobo, M. Tsapatsis, C.C. Freyhardt, S. Khodabandeh, P. Wagner, C.-Y. Chen, K.J. Balkus, S.I. Zones, M.E. Davis, J. Am. Chem. Soc. 119 (1997) 8474–8484.